Numerical calculation of transient excitonic Green functions in the presence of phonon scattering



1995 J. Phys.: Condens. Matter 7 4629

(http://iopscience.iop.org/0953-8984/7/24/005)

J. Phys.: Condens. Matter 7 (1995) 4629–4648. Printed in the UK

# Numerical calculation of transient excitonic Green functions in the presence of phonon scattering

Tadashi Takemori, Yoshikazu Motomura† and Masahiro Inoue
Institute of Applied Physics, University of Tsukuba, Tsukuba, Ibaraki 305, Japan

Received 11 October 1994, in final form 13 February 1995

**Abstract.** As a demonstration of the growing feasibility of quantum treatment of complex systems with parallel computing, we have performed a transient population dynamics calculation for carriers interacting via Coulomb and electron–phonon interactions. Two-point Keldysh functions are obtained by integrating the Dyson equation in the time domain. Keldysh functions are treated explicitly as matrices with discretized real time as their index in order to be able to deal squarely with fast transient phenomena. The Coulomb interaction is included in the electron self-energy within the Hartree–Fock approximation, while the interaction with localized non-dispersive thermal phonons is taken into account up to the second order in the electron–phonon vertex. The numerical procedure is applied to the case of carrier excitation by an ultrashort laser pulse in a model two-band semiconductor to obtain the transient behaviour of carrier population and the luminescence spectrum shortly after the excitation.

## 1. Introduction

The development in the laser technique involving ultrashort pulses has pushed the experimental time resolution down to femtoseconds, and an observation of very fast transient processes has now become feasible. The technique has recently been applied to probe the behaviour of the electronic system in semiconductors both in the bulk and in nanostructures (see e.g. Schmitt-Rink *et al* 1985, Chemla *et al* 1987, Knox *et al* 1985, Wake *et al* 1992, Yoon *et al* 1992, Rota *et al* 1993). If the recombination rate is slow, the electrons and holes created at a high energy by the laser pulse lose energy first via LO phonon emission. Coulomb scattering between carriers also assists in the rapid thermalization when the density of the excited carriers is high (Rota *et al* 1993, El Sayed *et al* 1994). This initial stage of thermalization takes place typically within a fraction of a picosecond. After the carriers have been scattered into states of small momentum, the interaction with acoustic phonons becomes important in the energy exchange with the environment. The carrier distribution then moves towards the thermal equilibrium, which is a slower process taking typically tens to hundreds of picoseconds (Inoue and Hanamura 1976a).

Based on the Hartree–Fock approximation to the self-energy in the Keldysh Green function scheme, Glutsch and Zimmermann (1992) recently calculated the transient behaviour of excitons shortly after the pump laser is turned on. The result revealed a highly non-linear behaviour of carrier population as a function of time, laser frequency, laser intensity and the smoothness of the onset of the laser beam. In particular, the population was shown to vary rapidly with time, and a transition to an excitonic phase was predicted at laser frequencies above the exciton level if the laser intensity is sufficiently low depending

† Present address: Fujitsu Ltd, Kawasaki, Kanagawa 211, Japan

0953-8984/95/244629+20$19.50  

on the smoothness of the laser onset. The population dynamics, however, did not include the energy exchange with phonons. As the Coulomb interaction is instantaneous, the equation of motion took on the form of the Heisenberg equation for each point in the momentum space so that each electron had to conserve its momentum.

Concerning the electron–phonon scattering, on the other hand, it was once customary to make a Markovian approximation and recast the problem in the form of a classical master equation (see e.g. Inoue and Hanamura 1976a). Although such a semi-classical approach has been applied to the analysis of fast transient processes (Kuhn and Rossi 1992, Rota *et al* 1993), it has its limitations. It is unclear, for example, how the uncertainty relation between time and energy should be incorporated. The non-equilibrium Green function method, on the other hand, allows the fully quantum mechanical incorporation of electron–phonon interaction into the population dynamics (see e.g. Haug and Koch 1990). Based on the generalized Kadanoff–Baym *ansatz* to express the time-ordered propagators in terms of the density matrix and the retarded Green functions, a self-consistent theory is obtained by assuming an exponential behaviour in time with a complex frequency for the retarded Green functions (Wigner–Weisskopf approximation), and then by determining the frequency to be consistent with the second-order self-energy. Tran Thoai and Haug (1993) used this scheme to obtain the transient behaviour of carriers under the influence of both excitonic interaction (Hartree–Fock exchange term) and electron–phonon interaction shortly after being excited by an ultrashort laser pulse. Their calculation and a subsequent work by Schilp *et al* (1994) using a density matrix formulation revealed a quantum beat of polarization with phonon frequency which was absent in a Markovian treatment and which was enhanced by the excitonic effect. While the Wigner–Weisskopf approximation in conjunction with the Kadanoff–Baym *ansatz* is valid when the rate of change of population and polarization is slow compared to the emission rate of phonons, it cannot be justified on general grounds in the case of fast transient phenomena where the population and polarization vary within the decay time of the retarded Green functions, thus influencing the time development of these functions.

In this paper, we present a quantum mechanical calculation of the transient population dynamics for carrier excitation in a two-band model, where the Coulomb interaction is treated in the Hartree–Fock approximation, the electron–phonon interaction is treated up to the second order in the interaction vertex, and where the two-point Keldysh function of electrons is calculated numerically as a matrix with discretized real time as its index without making any further assumptions as to their temporal behaviour. Such a treatment of population dynamics would have overwhelmed the computational capacity of a conventional machine. With the recent development of massively parallel computing, however, a full treatment of such problems on a quantum mechanical basis is becoming feasible. The present work is one such attempt. A very similar treatment of two-point Keldysh functions fully as a matrix in the time domain has been made also by Hartmann and Schäfer (1992) although without the Coulomb interaction. The present calculation may be regarded as the extension of their work to include the mean-field Hartree–Fock exchange term. The size of the calculation is also much larger: the number of $k$-points is more than doubled, and the number of time steps within the memory depth is nearly 5.6 times as many. A small time step and fine mesh in $k$-space are necessary to deal with the persistent oscillation of population and polarization caused by the Coulomb exchange term.

## 2. Preliminaries—formulation in the Keldysh scheme

### *2.1. Model*

Denoting the electron and phonon operators by $\tilde{C}$ and $b$, we take the model Hamiltonian as follows:

$$\tilde{H} = \sum_{\alpha,k} \varepsilon_\alpha(k)\tilde{C}^\dagger_{\alpha,k}\tilde{C}_{\alpha,k} + \sum_q \omega_q b^\dagger_q b_q - \sum_{\omega_p} \mu E(t)\left(\mathrm{e}^{-\mathrm{i}\omega_p t}\tilde{C}^\dagger_{1,k}\tilde{C}_{2,k} + \mathrm{e}^{\mathrm{i}\omega_p t}\tilde{C}^\dagger_{2,k}\tilde{C}_{1,k}\right)$$
$$+ \frac{1}{2}\sum_{\alpha,\beta}\sum_{k,k',q} V(q)\tilde{C}^\dagger_{\alpha,k+q}\tilde{C}^\dagger_{\beta,k'-q}\tilde{C}_{\beta,k'}\tilde{C}_{\alpha,k}$$
$$+ \sum_{\alpha,k,q} \gamma_\alpha(k+q,q)\left(b_q + b^\dagger_{-q}\right)\tilde{C}^\dagger_{\alpha,k+q}\tilde{C}_{\alpha,k}. \tag{1}$$

The first term is the unperturbed dispersion of the conduction band ($\alpha = 1$) and the valence band ($\alpha = 2$). The electron spin is neglected for the sake of simplicity. (Under qualifications, what follows may be regarded as dealing only with singlet excitons.) The second term is the phonon energy. The third term describes in the so-called 'rotating wave approximation', the interaction of electrons with a classical pump field whose frequency is centred around $\omega_p$ and whose envelope function is given by $E(t)$. The fourth term is the Coulomb interaction between carriers in a semiconductor, where an unscreened form

$$V(q) = 4\pi\mathrm{e}^2/\epsilon q^2 \tag{2}$$

is assumed with a background dielectric constant $\epsilon$. Hereafter, we shall assume that the effect of Hartree potential together with that of the charge compensating positive background is included in the one-particle energy $\varepsilon_\alpha(k)$. The last term is the electron–phonon interaction. In our calculation where a quantitative comparison with experiment is still out of the question, we shall satisfy ourselves with a separable form

$$|\gamma_\alpha(k_1,k_2)|^2 = g(k_1)g(k_2) \tag{3}$$

instead of the usual Fröhlich-type interaction

$$|\gamma_\alpha(k_1,k_2)|^2 \propto \frac{1}{|k_1-k_2|^2} \tag{4}$$

which is more appropriate for LO phonons. A separable form greatly reduces the computation load. We shall drop the dependence of $\gamma_\alpha(k_1,k_2)$ on $\alpha$ for the sake of simplicity. We shall also assume a simple functional form

$$g(k) = g_0 \exp\left\{-(k/k_c)^2\right\} \tag{5}$$

which is smoothly cut off at large values of $|k|$. In a realistic simulation of a material, the cut-off momentum $k_c$ (in fact the functional form of $\gamma_\alpha(k_1,k_2)$) will have to be determined from the knowledge of the dependence of the matrix element on $k$ in the momentum space. In the absence of such a knowledge, and also considering the qualitative nature of the present calculation, we have chosen $k_c$ to be 7.5 times the inverse Bohr radius of an exciton.

Both bands are taken to be parabolic with masses $m_e$ and $m_h$;

$$\varepsilon_1(k) = \frac{k^2}{2m_e} + E_g \qquad \varepsilon_2(k) = -\frac{k^2}{2m_h} \tag{6}$$

where $E_g$ is the band gap which is assumed to be large compared to the temperature, exciton binding energy or the reciprocal of the time scale of population dynamics. In accordance with this idea of a hierarchy of energy scales, we have excluded interband transition terms from all but the third term in the Hamiltonian (1). As a result, the problem can be reformulated in such a way that $E_g$ or $\omega_p$ (which is close to $E_g$) never appear explicitly in the theory. This is done by defining new electron operators

$$\begin{aligned} C_{1,k}(t) &= \tilde{C}_{1,k}(t)e^{i\omega_p t} \qquad C^\dagger_{1,k}(t) = \tilde{C}^\dagger_{1,k}(t)e^{-i\omega_p t} \\ C_{2,k}(t) &= \tilde{C}_{2,k}(t) \qquad C^\dagger_{2,k}(t) = \tilde{C}^\dagger_{2,k}(t) \end{aligned} \tag{7}$$

and by re-expressing the wave function of the system

$$|\psi(k,t)\rangle = \sum_{n,m} \sum_{\{\alpha\},\{k\}\{q\}} F_{n,m}(\{k\},\{q\},t) C^\dagger_{\alpha_1,k_1}(t) \ldots C^\dagger_{\alpha_n,k_n}(t) b^\dagger_{q_1} \ldots b^\dagger_{q_m} |0\rangle \tag{8}$$

in terms of the new operators. The Schrodinger equation will then read

$$i\frac{\partial}{\partial t}|\psi(k,t)\rangle = \left(\tilde{H} - \omega_p n_1\right)|\psi(k,t)\rangle \equiv H|\psi(k,t)\rangle \tag{9}$$

with a new Hamiltonian

$$\begin{aligned} H = \tilde{H} - \sum_k \omega_p C^\dagger_{1,k} C_{1,k} &= \sum_k \left[\varepsilon_1(k) - \omega_p\right] C^\dagger_{1,k} C_{1,k} + \sum_k \varepsilon_2(k) C^\dagger_{2,k} C_{2,k} + \sum_q \omega_q b^\dagger_q b_q \\ &- \sum_{\omega_p} \mu E(t) \left(C^\dagger_{1,k} C_{2,k} + C^\dagger_{2,k} C_{1,k}\right) + \frac{1}{2} \sum_{\alpha,\beta} \sum_{k,k',q} V(q) C^\dagger_{\alpha,k+q} C^\dagger_{\beta,k'-q} C_{\beta,k'} C_{\alpha,k} \\ &+ \sum_{\alpha,k,q} \gamma(k+q,k) \left(b_q + b^\dagger_{-q}\right) C^\dagger_{\alpha,k+q} C_{\alpha,k} \end{aligned} \tag{10}$$

which describes a system of a reduced band gap illuminated by the pump field whose central frequency is zero. We shall hereafter work with this reduced Hamiltonian (10).

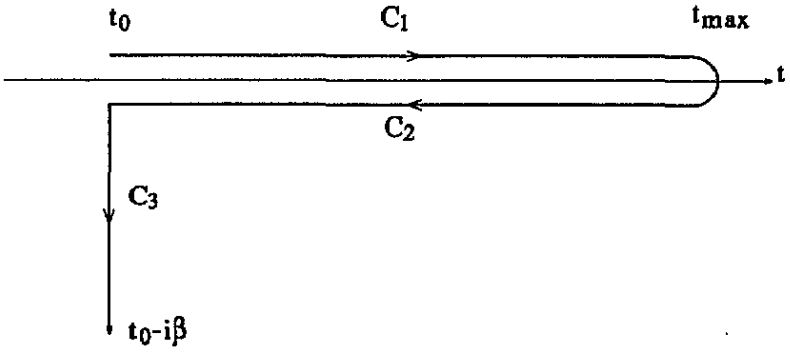


**Figure 1.** Integration path in the complex time domain.

### 2.2. *Keldysh functions*

Let us now briefly summarize the method of non-equilibrium Green functions (Keldysh 1965) bearing in mind the simplifications that arise in the present case of a transient carrier excitation (Schäfer and Treusch 1986, Schäfer 1987, Haug 1987, Schmitt-Rink and Chemla 1986, Schmitt-Rink *et al* 1988) in an intrinsic semiconductor whose band gap is large compared to the temperature. The Keldysh Green function is defined as the expectation value of a 'time-ordered' product of operators

$$\hat{G}(\tau_1, \tau_2, \ldots, \tau_n) = \langle T_C O_1(\tau_1) O_2(\tau_2) \ldots O_n(\tau_n) \rangle \tag{11}$$

whose ordering is defined along a contour $C$ on the complex time plane as shown in figure 1. The path starts from the initial time $t_0$ when the system is considered to be in thermal equilibrium, then proceeds along the real axis to a time $t_{\max}$ larger than any external time variable of the $n$-point function to be calculated ($C_1$ of figure 1), then returns to the initial time $t_0$ ($C_2$ of figure 1), and then proceeds in the direction of the negative imaginary time ($C_3$ of figure 1), ending up at the time $t_0 - \mathrm{i}\beta$. To indicate a position on the contour $C$, we shall use a variable $\tau$ which is taken to increase along the length of the path $C$. A variable $t$ shall be used to indicate the time coordinate of the point specified by the variable $\tau$ (e.g. symbols $t$, $t'$, $t_1$ and $t_2$ shall indicate the time coordinate of points $\tau$, $\tau'$, $\tau_1$ and $\tau_2$). Thus, $t$ increases with $\tau$ ($\mathrm{d}t = \mathrm{d}\tau$) on $C_1$, while $t$ decreases with $\tau$ ($\mathrm{d}t = -\mathrm{d}\tau$) on $C_2$ and $t(\tau) - t_0$ is pure imaginary ($\mathrm{d}t = -\mathrm{i}\,\mathrm{d}\tau$) when $\tau$ indicates a point on $C_3$. Taking the free-particle part (the first two terms in (8)) as the unperturbed Hamiltonian

$$H_0 = \sum_k \left(\varepsilon_1(k) - \omega_p\right) C^\dagger_{1,k} C_{1,k} + \sum_k \varepsilon_2(k) C^\dagger_{2,k} C_{2,k} + \sum_q \omega_q b^\dagger_q b_q \tag{12}$$

and denoting by $H_{\mathrm{int}}$ the remaining terms of the Hamiltonian in the interaction representation

$$H_{\mathrm{int}} = -\sum_{\omega_p} \mu E(t) \left( C^\dagger_{1,k} C_{2,k} + C^\dagger_{2,k} C_{1,k} \right) + \frac{1}{2} \sum_{\alpha,\beta} \sum_{k,k',q} V(q) C^\dagger_{\alpha,k+q} C^\dagger_{\beta,k'-q} C_{\beta,k'} C_{\alpha,k}$$
$$+ \sum_{\alpha,k,q} \gamma(k+q,k) \left( b_q + b^\dagger_{-q} \right) C^\dagger_{\alpha,k+q} C_{\alpha,k} \tag{13}$$

the definition of the two-point function can be written as

$$G_{\alpha,\beta}(k,t,t') = \frac{\langle T_c(S_c C_{\alpha,k}(t) C^\dagger_{\beta,k}(t')) \rangle_0}{\langle T_c(S_c) \rangle_0} \equiv \frac{\mathrm{Tr}[\mathrm{e}^{-\beta H_0} T_c(S_c C_{\alpha,k}(t) C^\dagger_{\beta,k}(t'))]}{\mathrm{Tr}[\mathrm{e}^{-\beta H_0} T_c(S_c)]} \tag{14}$$

where

$$S_c = \exp\left( -\mathrm{i} \int_c \mathrm{d}t(\tau) H_{\mathrm{int}}(\tau) \right). \tag{15}$$

The integration along $C_3$ ensures that the system is in thermal equilibrium at $t_0$ under the interaction Hamiltonian. Fortunately for the present model with a large $E_g$, this piece of integration can be omitted, since the external field is switched on only after $t_0$, and also because the equilibrium state of $H_0$ without any carriers and with thermal phonons is already the equilibrium state of $H_0 + H_{\mathrm{int}}$ at $t_0$. The integration will therefore be along $C_1$ and $C_2$ only. Defining the multiplication of two (infinite-dimensional) matrices with time and band indices $A_{\alpha,\gamma}(\tau_1, \tau_3)$ and $B_{\gamma,\beta}(\tau_3, \tau_2)$ as

$$(A * B)_{\alpha,\beta}(\tau_1, \tau_2) = \sum_\gamma \int_c A_{\alpha,\gamma}(\tau_1, \tau_3) B_{\gamma,\beta}(\tau_3, \tau_2)\, \mathrm{d}t_3 \tag{16}$$

where

$$dt_3 = dt(\tau_3) = \frac{dt_3}{d\tau_3} d\tau_3 = \begin{cases} d\tau_3 & \text{on } C_1 \\ -d\tau_3 & \text{on } C_2 \end{cases} \tag{17}$$

the electron self-energy is defined as

$$i\Sigma_{\alpha,\beta}(k, \tau_1, \tau_2) = [G0^{-1}]_{\alpha,\beta}(k, \tau_1, \tau_2) - [G^{-1}]_{\alpha,\beta}(k, \tau_1, \tau_2) \tag{18}$$

where

$$G0_{\alpha,\beta}(k, \tau_1, \tau_2) = \left[\left\{\frac{d}{dt_1} + i\varepsilon_\alpha(k)\right\}\delta(\tau_1 - \tau_2)\delta_{\alpha,\beta}\right]^{-1} \tag{19}$$

is the Green function of the free-particle Hamiltonian $H_0$. Multiplying (18) by $G$ from the right or from the left, one obtains

$$i\frac{d}{dt_1}G_{\alpha,\beta}(k, \tau_1, \tau_2) = \varepsilon_\alpha(k)G_{\alpha,\beta}(k, \tau_1, \tau_2) + \sum_\gamma \int_c \Sigma_{\alpha,\gamma}(k, \tau_1, \tau_3)G_{\gamma,\beta}(k, \tau_3, \tau_2)\, dt_3 + i\delta(\tau_1 - \tau_2)\delta_{\alpha,\beta} \tag{20}$$

$$i\frac{d}{dt_2}G_{\alpha,\beta}(k, \tau_1, \tau_2) = -\varepsilon_\beta(k)G_{\alpha,\beta}(k, \tau_1, \tau_2) - \sum_\gamma \int_c G_{\alpha,\gamma}(k, \tau_1, \tau_3)\Sigma_{\gamma,\beta}(k, \tau_3, \tau_2)\, dt_3 - i\delta(\tau_1 - \tau_2)\delta_{\alpha,\beta}. \tag{21}$$

This can be regarded as the equation of motion for $G$ provided the self-energy $\Sigma$ is given as an explicit functional of $G$.

The integration over $t_3$ in (16), (20) and (21) need not be taken from $t_0$ to $t_{max}$ but only up to whichever is larger of $t(\tau_1)$ and $t(\tau_2)$. This is so because the integrations over $\tau_3$ along the pieces of $C_1$ and $C_2$ where $t_3 > \max\{t(\tau_1), t(\tau_2)\}$ exactly cancel each other, since $dt_3|_{C_1} = -dt_3|_{C_2}$ and $G_{\alpha\gamma}(k, \tau_1, \tau_3)$, $G_{\gamma\beta}(k, \tau_3, \tau_2)$, $\Sigma_{\alpha\gamma}(k, \tau_1, \tau_3)$ and $\Sigma_{\gamma\beta}(k, \tau_3, \tau_2)$ depend only on $t(\tau_3)$ irrespective of whether $\tau_3$ is on $C_1$ or $C_2$. This last fact follows directly from the definition of $G_{\alpha\beta}(k, \tau_1, \tau_3)$ and $\Sigma_{\alpha\beta}(k, \tau_1, \tau_3)$. By recursively applying the argument, one concludes that the same holds true, however complicated the diagram; i.e. that in integrating over the position of an intermediate vertex along the contour $C$, the time variable need not be taken beyond the largest of the external time variables of the $n$-point function. The consequence of this is that, whatever diagrammatic representation one assumes for $\Sigma$, the time evolution of $G_{\alpha\beta}(k, \tau_1, \tau_2)$ can be calculated solely from the knowledge of $G_{\alpha\beta}(k, \tau_3, \tau_4)$ with $\max\{t(\tau_3), t(\tau_4)\} \leqslant \max\{t(\tau_1), t(\tau_2)\}$.

### *2.3. Self energy*

An approximation to $\Sigma$ as a functional of $G$ is obtained if one notices that the usual diagrammatic rules for $T$ products also apply here (Lifshitz and Pitaevskii 1981, Rammer and Smith 1986), so that the self-energy is identified with the set of one-electron-irreducible diagrams. If we take the Hartree–Fock exchange diagram for Coulomb interaction and the second-order diagram for electron–phonon interaction as shown in figure 2, the self-energy is given by

$$\Sigma_{\alpha,\beta}(k, \tau_1, \tau_2) = -\mu\{E(t_1)\delta_{\alpha,1}\delta_{2,\beta} + E(t_1)^*\delta_{\alpha,2}\delta_{1,\beta}\}\delta(\tau_2 - \tau_1) + \sum_{k'} V(k - k')\{G_{\alpha,\beta}(k', \tau_1, \tau_1 + 0) - \delta_{\alpha,2}\delta_{\beta,2}\}\delta(\tau_2 - \tau_1) - i\sum_{k'} g(k)g(k')D(k - k', \tau_1, \tau_2)G_{\alpha,\beta}(k', \tau_1, \tau_2) \tag{22}$$

where $D$ is the Green function for phonons,

$$D(q, \tau_1, \tau_2) = \langle T_c u_q(\tau_1) u_{-q}(\tau_2) \rangle \tag{23}$$

$$u_q(\tau) \equiv b_q(\tau) + b^{\dagger}_{-q}(\tau). \tag{24}$$

The equilibrium valence electron contribution is subtracted from the exchange energy term in (22), since such a contribution can be included in the renormalized band energy $\varepsilon_\alpha(k)$. On the other hand, the phonon term is left as it is, so that the band energy renormalization due to electron–phonon interaction has to be taken into account in interpreting the numerical results.

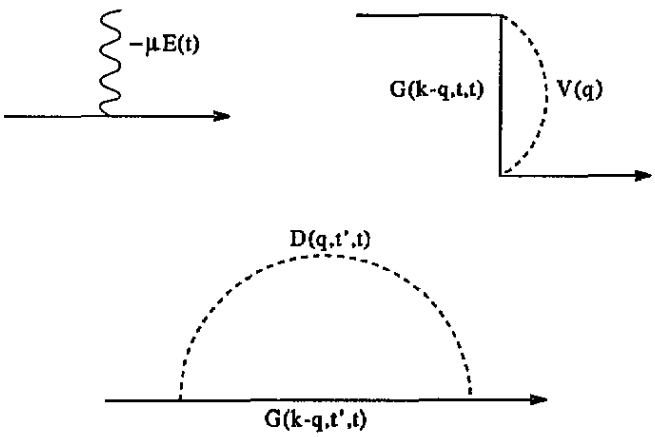


**Figure 2.** Self-energy diagrams.

As pointed out by El Sayed *et al* (1994), the use of parabolic bands in combination with bare Coulomb interaction (2) leads to an ill defined exchange term because of the contribution from large values of $|k|$. In the present calculation, this manifests itself in the dependence of the solution on the cut-off momentum in the $k$-space integration. Here again, the $k$-space integration cannot be unlimited in reality, and has to be cut off somewhere. We have done this by introducing the same smooth cut-off factor

$$V(k-k') \rightarrow V(k-k') \exp\left\{-(k/k_c)^2\right\} \exp\left\{-\left(k'/k_c\right)^2\right\} \tag{25}$$

as for the phonon vertex.

A similar set of equations may be set up for $D$ to be solved simultaneously with the equations for $G$. Instead, we shall here assume, for the sake of simplicity, the unperturbed thermal phonons

$$D(q, \tau_1, \tau_2) = n_q \left\{\exp[-i\omega_q(t_1 - t_2)] + \exp[i\omega_q(t_1 - t_2)]\right\} + \theta(\tau_1 - \tau_2)\exp[-i\omega_q(t_1 - t_2)] + \theta(\tau_2 - \tau_1)\exp[i\omega_q(t_1 - t_2)] \tag{26}$$

where $n_q$ is the Bose distribution function

$$n_q = \langle b^{\dagger}_q b_q \rangle = \frac{1}{e^{\beta\omega_q} - 1}. \tag{27}$$

This approximation to $D$ is well justified for carrier excitation in a semiconductor where the LO phonons are not expected to be affected strongly by the population of carriers.

### *2.4. Luminescence and absorption*

Let us give an expression of luminescence intensity in terms of the electron Green functions when the radiative recombination rate is small. For each mode of radiation of frequency $\omega$, we shall assume a Hamiltonian

$$H_{\rm rad}(\omega) + H_{\rm lum}(\omega) \equiv \omega a_\omega^\dagger a_\omega + \sum_k \left\{ \eta P_k a_\omega^\dagger + {\rm cc} \right\} \tag{28}$$

where $a_\omega$ is the photon operator,

$$P_k(t) \equiv C_{1,k}^\dagger C_{2,k} \tag{29}$$

is the polarization, the momentum of the radiation is neglected compared to the crystal momentum, the electronic transition associated with photon emission/absorption is assumed to be local, and the rotating wave approximation is used again. If this is included in the Hamiltonian of the system, the photon number at time $T$ is given by

$$N_\omega(T) = \langle a_\omega^\dagger(T) a_\omega(T) \rangle = \frac{{\rm Tr}[\exp(-\beta H_0) T_{\rm c} S_{\rm c} S_{\rm lum} a_\omega^\dagger(T) a_\omega(T)]}{{\rm Tr}[\exp(-\beta H_0)]} \tag{30}$$

where $S_{\rm c}$ now includes $H_{\rm rad}$ in its time evolution

$$S_{\rm c} = \exp\left\{ -{\rm i} \int_{C_1+C_2} (H_{\rm int} + H_{\rm rad})\, {\rm d}t(\tau) \right\} \tag{31}$$

and

$$S_{\rm lum} = \exp\left\{ -{\rm i} \int_{C_1+C_2} (H_{\rm lum})\, {\rm d}t(\tau) \right\}. \tag{32}$$

The trace has to be taken over states with no photons in accordance with the assumption of a large $E_{\rm g}$, and the contour $C$ should run only up to time $T$ and return. Expanding $S_{\rm lum}$ to the first order in $H_{\rm lum}$ and making contraction of the photon operators according to

$$\langle T_{\rm c} a_\omega(\tau_1) a_\omega^\dagger(\tau_2) \rangle = \theta(\tau_1 - \tau_2) \exp[-{\rm i}\omega(t_1 - t_2)] \tag{33}$$

one obtains

$$N_\omega(T) = |\eta|^2 \int_{C_1}^T {\rm d}\tau_1 \int_{C_2}^T {\rm d}\tau_2 \sum_{k,k'} \langle T_C P_{k'}^\dagger(\tau_2) P_k(\tau_1) \rangle {\rm e}^{{\rm i}\omega(t_2 - t_1)} \tag{34}$$

for a single mode of radiation with frequency $\omega$. In reality, any observation is of finite energy resolution, so that a more relevant quantity will be the number of photons within a certain range $\delta_{\rm res}$ of a frequency $\omega_{\rm c}$. A convenient candidate would then be

$$N_{\omega_{\rm c}}(T) = \int N_\omega(T) {\rm d}\omega \frac{\delta_{\rm res}^2}{(\omega - \omega_{\rm c})^2 + \delta_{\rm res}^2} = \pi |\eta|^2 \delta_{\rm res} \int_{C_1}^T {\rm d}\tau_1 \int_{C_2}^T {\rm d}\tau_2 \sum_{k,k'} \langle T_C P_{k'}^\dagger(\tau_2) P_k(\tau_1) \rangle$$
$$\times \exp\{{\rm i}\omega_{\rm c}(t_2 - t_1)\} \exp\{-\delta_{\rm res}|t_2 - t_1|\}. \tag{35}$$

whose rate of change is given by

$$R(t) \equiv {\rm d}N_\omega(t)/{\rm d}t = 2\pi\delta_{\rm res}|\eta|^2 {\rm Re}\left[ \int_C^t \sum_{k,k'} \langle T_C P_{k'}^\dagger(\tau') \cdot P_k(\tau) \rangle \right.$$
$$\left. \times \exp\left\{{\rm i}\omega_{\rm c}(t' - t)\right\} \exp\left\{-\delta_{\rm res}|t' - t|\right\} {\rm d}\tau' \right]. \tag{36}$$

One has to be careful in interpreting this quantity in relation to the experimentally observed transient spectrum intensity (Eberly and Wodkiewitz 1977, Khiznyakov and Rebane 1978)†. The formula (36) corresponds to what is called the 'Page–Lampard' power spectrum and does not correspond to a physical readout of most frequency-resolved experiments. It can even become temporarily negative as a result of the uncertainty principle. An expression corresponding to experimental result will have to be based on the analysis of the experimental set-up. Broadly speaking, however, an experimental readout may be regarded as an average of (36) over a period $1/2\delta_{\rm res}$ with a damping factor $2\delta_{\rm res}$. This can be seen as follows: if the experiment is such that a detector monitors the photon field intensity behind a Lorentz filter of frequency resolution $\delta_{\rm res}$, the readout at time $T$ will be proportional to the intensity of the photon field at the detector at time $T$. The amplitude of the field is the accumulation over time $t$ ($< T$) of photon field amplitude before the filter multiplied by the filter response function $\exp\{i\omega_c(T-t)\}\exp\{-\delta_{\rm res}|T-t|\}$. The readout at time $T$ will then be proportional to

$$2\pi(\delta_{\rm res})^2|\eta|^2\int_{C_1}^{T}{\rm d}\tau_1\int_{C_2}^{T}{\rm d}\tau_2\sum_{k,k'}\langle T_C P_{k'}^{\dagger}(\tau_2)P_k(\tau_1)\rangle$$
$$\times\exp\{i\omega_c(t_2-t_1)\}\exp\{-\delta_{\rm res}|T-t_1|\}\exp\{-\delta_{\rm res}|T-t_2|\}. \tag{37}$$

This has the advantage of being positive definite. The relation

$$\langle P_{k'}^{\dagger}(t_2)P_k(t_1)\rangle = \langle P_k^{\dagger}(t_1)P_{k'}(t_2)\rangle^*. \tag{38}$$

allows us to rewrite (37) as

$$2\delta_{\rm res}\int_{-\infty}^{T}R(t)\exp(-2\delta_{\rm res}|T-t|)\,{\rm d}t \tag{39}$$

i.e. the accumulation of $R(t)$ over time up to $T$ with a damping constant $2\delta_{\rm res}$.

An approximation has to be made to the four-point function in the integrand. In line with the mean-field approximation, we shall use the substitution

$$\langle T_C P_{k'}^{\dagger}(\tau')\cdot P_k(\tau)\rangle \equiv \langle T_c C_{1,k}^{\dagger}(\tau)C_{2,k}(\tau)C_{2,k'}^{\dagger}(\tau')C_{1,k'}(\tau')\rangle$$
$$\to \langle T_c C_{1,k}^{\dagger}(\tau)C_{1,k'}(\tau')\rangle\langle T_c C_{2,k}(\tau)C_{2,k'}^{\dagger}(\tau')\rangle$$
$$+\langle T_c C_{1,k}^{\dagger}(\tau)C_{2,k}(\tau)\rangle\langle T_c C_{2,k'}^{\dagger}(\tau')C_{1,k'}(\tau')\rangle$$
$$= -G_{11}(k,\tau',\tau)G_{22}(k,\tau,\tau')\delta_{k,k'}+G_{21}(k,\tau,\tau+0)G_{12}(k',\tau',\tau'+0). \tag{40}$$

The second term on the RHS corresponds to the emission that is coherent with the pump light, whose interference with the pump light should also account for the pump light absorption. The first term, on the other hand, corresponds to the incoherent emission that is proportional to the product of quasielectron and quasihole density in the $k$ space. The delta function $\delta_{k,k'}$ derives from the long-wavelength limit of radiation, and should in reality have a resolution of the order of the radiation momentum. The appearance of this delta function is also a sign of the incoherent nature of the first term. In the light of the different nature of the two terms, we shall hereafter treat them separately.

† The authors are indebted to one of the anonymous referees for pointing out the non-trivial relationship between the photon number spectrum and the experimental measurement of the transient spectrum.

The expression for the absorption rate can be obtained in a similar fashion, this time starting at $t_0$ with states with one photon of frequency $\omega$ and taking a trace over no photon states at time $T$. The probability that the photon has been absorbed by the time $T$ is then given by

$$P_{\mathrm{abs}}(T) = \frac{\mathrm{Tr}_1[\exp(-\beta H_0) T_C S_c S_{\mathrm{lum}} P_0(T)]}{\mathrm{Tr}_1[\exp(-\beta H_0)]} \tag{41}$$

where $\mathrm{Tr}_1[]$ denotes the trace over one-photon states at time $t_0$, and $P_0$ is the projection onto no photon states. Expanding again to the lowest order in $|\eta|$, one may thus be tempted to define the rate of absorption as

$$\begin{aligned} A(t) \equiv \frac{\mathrm{d}P_{\mathrm{abs}}(t)}{\mathrm{d}t} &= \frac{2|\eta|^2}{\pi}\mathrm{Re}\Bigg[\int_{C_1}^{t} \sum_{k,k'} \langle C^{\dagger}_{2,k}(\tau) C_{1,k}(\tau) C^{\dagger}_{1,k'}(\tau') C_{2,k'}(\tau')\rangle \\ &\quad \times \exp\left\{-\mathrm{i}\omega_c(t'-t)\right\} \exp\left\{-\delta_{\mathrm{res}}|t'-t|\right\} \mathrm{d}\tau'\Bigg] \\ &= \frac{2|\eta|^2}{\pi}\mathrm{Re}\Bigg[\int_{C_1}^{t} \sum_{k} (-1) G_{22}(k,t,t') G_{11}(k,t',t) \\ &\quad \times \exp\left\{-\mathrm{i}\omega_c(t'-t)\right\} \exp\left\{-\delta_{\mathrm{res}}|t'-t|\right\} \mathrm{d}\tau' \\ &\quad + \sum_{k} G_{21}(k,t,t) \int_{C_1}^{t} \sum_{k'} G_{12}(k',t',t') \exp\left\{-\mathrm{i}\omega_c(t'-t)\right\} \\ &\quad \times \exp\left\{-\delta_{\mathrm{res}}|t'-t|\right\} \mathrm{d}\tau'\Bigg] \end{aligned} \tag{42}$$

after averaging over a frequency range around $\omega_c$ with a Lorentzian of width $\delta_{\mathrm{res}}$ as in (36). The interpretation of (42) in terms of experimental observation is even more complicated than for luminescence. If we consider the readout of a detector behind a filter as before, and suppose that the system is exposed to incoherent diffuse white light of intensity $I_0$ independent of frequency, the detector readout at time $t$ will be larger (by an amount $\delta I(t)$ proportional to $I_0$) compared to the case without the incoherent diffuse background. A tentative definition of the transient absorption spectrum would be

$$A(t) = \lim_{I_0 \to 0} \frac{I_0 - \delta I(t)}{I_0}. \tag{43}$$

In the case of a Lorentzian filter, the same argument as for the luminescence leads to the expression for transient absorption

$$2\delta_{\mathrm{res}} \int_{-\infty}^{T} A(t) \exp(-2\delta_{\mathrm{res}}|T-t|)\, \mathrm{d}t \tag{44}$$

to the lowest order of $\eta$.

### *2.5. Numerical implementation*

Let us briefly comment on the actual implementation of the numerical procedure on the parallel computer AP1000 which consists of a host processing unit and up to 1024 cell processing units. The time evolution of $G$ solved by discretizing the time variable and by integrating the equations of motion (20) and (21) according to the second-order Runge–Kutta scheme. The table of $G_{\alpha\beta}(k, \tau_1, \tau_2)$ with $\tau_1, \tau_2$ on the path $C_1$ of figure 1 has to be stored and its time evolution solved for each $|k|$. Denoting by $\sigma_1$ and $\sigma_2$ the points on $C_2$ that correspond to the same value of $t$ as $\tau_1$ and $\tau_2$ respectively, the Keldysh functions with either of the $\tau$ variables on $C_2$ are obtained by the relation

$$G_{\alpha\beta}(k, \sigma_1, \tau_2) = \begin{cases} G_{\alpha\beta}(k, \tau_1, \tau_2) & \text{if } \tau_1 \geqslant \tau_2 \\ G_{\beta\alpha}(k, \tau_2, \tau_1)^* & \text{if } \tau_1 < \tau_2 \end{cases}$$

$$G_{\alpha\beta}(k, \tau_1, \sigma_2) = \begin{cases} G_{\beta\alpha}(k, \tau_2, \tau_1)^* & \text{if } \tau_1 > \tau_2 \\ 1 + G_{\alpha\beta}(k, \tau_1, \tau_2) & \text{if } \tau_1 = \tau_2 \\ G_{\alpha\beta}(k, \tau_1, \tau_2) & \text{if } \tau_1 < \tau_2 \end{cases} \tag{45}$$

$$G_{\alpha\beta}(k, \sigma_1, \sigma_2) = \begin{cases} G_{\beta\alpha}(k, \tau_2, \tau_1)^* & \text{if } \tau_1 \neq \tau_2 \\ 1 + G_{\alpha\beta}(k, \tau_1, \tau_2) & \text{if } \tau_1 = \tau_2. \end{cases}$$

The momentum space is divided into shells according to the amplitude $|k|$, and each cell processing unit is assigned a shell for which to perform the task. The self-energy is compiled by the host processing unit at each step of integration from the data sent from the cells, and is then fed to cells for the next step of integration. We have tried running the program with 1024, 512, 256, 128, and 64 cells, but 128 cells proved to be the most practical choice for the present calculation with regard to accuracy and the computation time. The results in the next section are obtained with 128 cells.

Another point concerning the practicability of the calculation is the integration cut-off. As regards the integration in the momentum space when calculating the self-energy, we have employed a Gaussian cut-off not only in the separable form of the electron–phonon vertex but also for the each end of the Coulomb vertex. The cut-off momentum $k_c$ is taken in a region where electron/hole population and polarization are small (see figures 3, 5, and 6). A Gaussian cut-off is employed also in the time domain for the phonon function

$$D_c(q, \tau, \tau') = D(q, \tau, \tau') \exp\left\{-\left[\delta_D(t' - t)\right]^2\right\} \tag{46}$$

which may be regarded as giving a width $\delta_D$ to the phonon band. This ensures that the self energy $\Sigma_{\alpha,\beta}(k, \tau', \tau)$ also diminishes with $|t' - t|$ within the time scale $1/\delta_D$, thereby rendering the time integration in (20) and (21) convergent. The equation of motion can then be solved far into the future without retaining all the $G_{\alpha\beta}(k, \tau_1, \tau_2)$ since $t_0$.

## 3. Numerical results

Let us now present the numerical results. We have used material parameters that correspond to the bulk GaAs as listed in table 1. Hereafter, we shall employ the units such that the energy is in $(\mathrm{Ryd}^{\mathrm{ex}})^{-1}$ (the exciton binding energy), time is in 1 $(\mathrm{Ryd}^{\mathrm{ex}})^{-1}$, and the length is in $a_{\mathrm{B}}^{\mathrm{ex}}$ (the exciton Bohr radius). The carrier masses are then $m_e/\hbar^2 = 1.14\ (\mathrm{Ryd}^{\mathrm{ex}})^{-1}(a_{\mathrm{B}}^{\mathrm{ex}})^{-2}$ and $m_h/\hbar^2 = 8.14\ (\mathrm{Ryd}^{\mathrm{ex}})^{-1}(a_{\mathrm{B}}^{\mathrm{ex}})^{-2}$. The LO phonon energy listed in table 1 is 8.27 $(\mathrm{Ryd}^{\mathrm{ex}})$

and the phonon band width $\delta_D$ is taken to be a tenth of $\omega_q$. The pump laser pulse is assumed to be of the form

$$-\mu E(t) = W_0 \exp\left[-\{\delta_p(t-t_0)\}^2\right]\exp(-i\omega_p t). \tag{47}$$

We present the results for $W_0 = 0.02$ (Ryd$^{ex}$) and $W_0 = 0.20$ (Ryd$^{ex}$). Estimating the interband transition matrix element by $|M|^2 = m_0 E_g/6$ (Stern 1963), one obtains $\mu \simeq 0.04(a_B^{ex})^{2/3}$ (Ryd$^{ex}$)$^{1/2}$. Then the amplitude $W_0 = 0.02$ (Ryd$^{ex}$) can be attained by focusing a laser pulse of 50 MW peak power on an area of 1 mm$^2$.

**Table 1.** Parameters for GaAs.

| Parameter | Value |
|---|---|
| band gap ($E_g$) | 1.428 eV |
| electron effective mass ($m_e$) | $0.063m_0$ |
| hole effective mass ($m_h$) | $0.450m_0$ |
| LO phonon frequency ($\omega_q$) | 36.4 meV |
| exciton binding energy ((Ryd$^{ex}$)$^{-1}$) | 4.4 meV |
| exciton Bohr radius ($a_B^{ex}$) | 12.5 nm |
| time unit (1 (Ryd$^{ex}$)$^{-1}$) | 149.6 fs |

Figure 3 shows the time development of electron and hole population excited by a laser pulse of amplitude $W_0 = 0.02$ (Ryd$^{ex}$), bandwidth $\delta_p = 1.0$ (Ryd$^{ex}$), and central frequency $\hbar\omega_p = E_g + 24$ (Ryd$^{ex}$). The electron–phonon coupling strength is taken to be $\gamma(0,0) = 5.0 \times 10^{-2}$ (Ryd$^{ex}$). The ordinate is the carrier density in the $k$ space, so that after multiplying by the density of states and integrating over $k$, the total carrier number is conserved after the laser pulse has subsided. Three large peaks develop in the electron density profile on the lower-energy side of the initial peak. The temperature $k_BT = 5.88$ (Ryd$^{ex}$) (273 K) is too low for peaks to appear on the higher-energy side of the initial peak. The peaks at lower energy gradually overtake those at higher energies in size as the electrons give up energy to phonons with the progression of time. The energy separation between consecutive peaks is the LO phonon energy. The electron population eventually accumulates at small-momentum states. The hole population, on the other hand, does not show any prominent structure because of the large effective mass. The polarization $|P_k(t)|$ rises near resonance ($E = E_g + 24$ (Ryd$^{ex}$) with the arrival of the pump pulse, and then decays smoothly after the pump pulse has passed. The pump pulse used here is too long for the phonon quantum beats to manifest itself.

The electron migration to lower momentum is accompanied by the red shift of incoherent light emission, which is shown in figure 4 where the emission rate is plotted as a function of time for frequencies $E_g+24$ Ryd$^{ex}$, $E_g+16$ Ryd$^{ex}$, $E_g+8$ Ryd$^{ex}$, and $E_g$. The photon energy resolution is set to $\delta_{res} = 4$ Ryd$^{ex}$. The emission near the pump frequency rises rapidly on carrier excitation, reaching the peak value at about 0.8 (Ryd$^{ex}$)$^{-1}$ after the arrival of the pulse. The emission at $E_g + 24$ Ryd$^{ex}$ then diminishes rapidly with time before turning to a slower rate of decrease at about 2.4 (Ryd$^{ex}$)$^{-1}$ after the arrival of the pulse. The emission at $E_g + 16$ Ryd$^{ex}$ decreases more slowly than that at $E_g + 24$ Ryd$^{ex}$. On the other hand, luminescence at $E_g$ and $E_g + 8$ Ryd$^{ex}$ appears immediately on pulse excitation, and then continues to increase within the range of time calculated. This result compares well with the experimental result by Rota *et al* (1993). They compared their result to a Monte Carlo simulation where carrier scattering was treated classically as an instantaneous probabilistic process satisfying the energy conservation $E_f = E_i \pm \omega_{ph}$ with respect to the initial and final electron kinetic energy and the phonon frequency. The present calculation, on the other

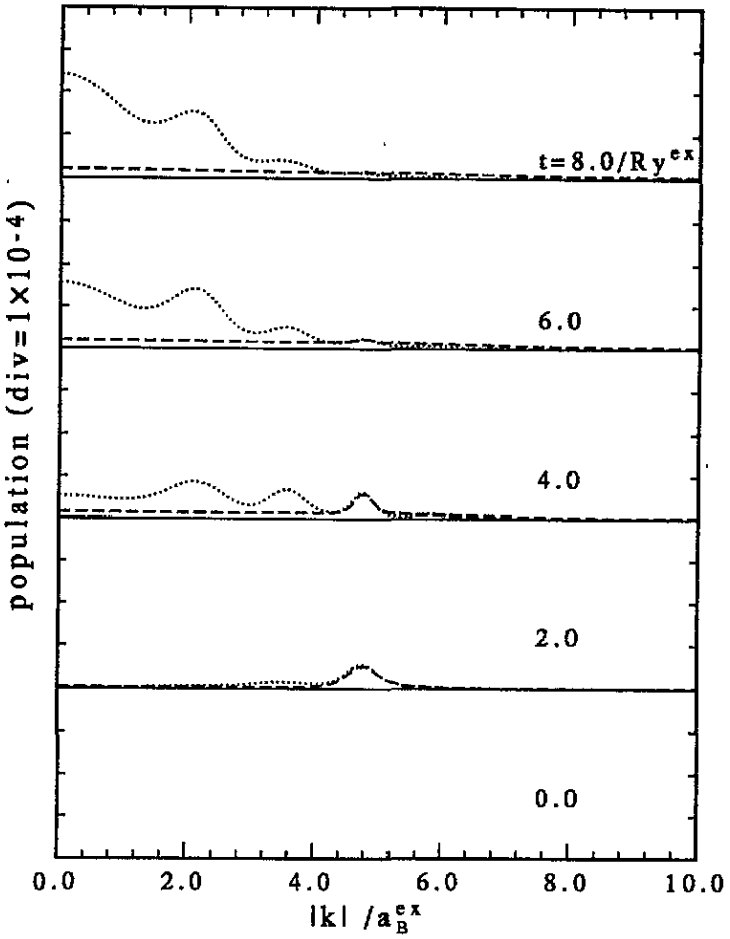


**Figure 3.** Variation with time of electron (·····) and hole (– – –) population after excitation by a laser pulse. The central pump laser frequency is $E_g + 24$ Ryd$^{ex}$, and the central phonon energy is 8.27 Ryd$^{ex}$.

hand, is fully quantum mechanical, so that the energy conservation and uncertainty relation are automatically taken care of.

There is a possibility that the Hartree–Fock exchange field (the so-called electron–hole internal field) sustains itself without being driven by a coherent laser field if sufficient number of carriers are excited and the temperature is kept low. The possibility of excitonic condensation has long been discussed (see e.g. Halperin and Rice 1968). In our approximation where the pump laser is treated as a classical field, the phenomenon is essentially the same as the emergence of an excitonic phase. The amplitude of the stationary solution of excitonic polarization $P_k(t) \equiv G_{12}(k, t, t)$ as a function of the external laser amplitude shows a hysteresis, and has a non-vanishing limit as the external laser amplitude tends to zero if the laser frequency is larger than the threshold for creating real excitons.

In fact, Butov *et al* (1994) have recently observed an evidence of an excitonic condensation in photoluminescence broad-band noise in AlAs/GaAs quantum wells. The actual process of the development of such a condensate is for the excited carriers to give up energy to phonons, excitons eventually accumulating at the lowest-energy state. The

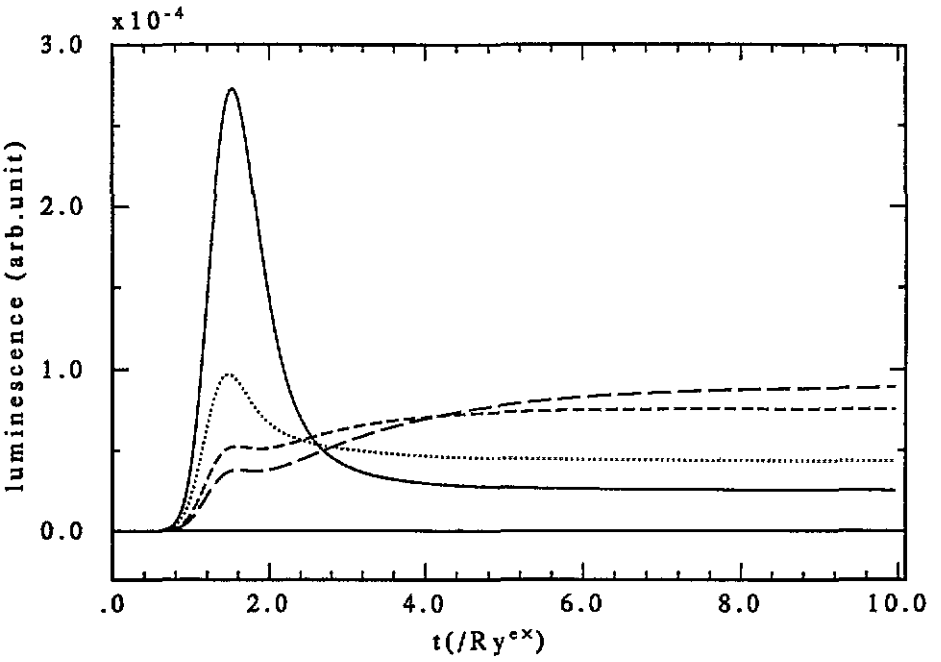


**Figure 4.** Frequency-resolved incoherent luminescence emission rates as functions of time. Pump laser pulse is centred at $t = 3.0$ (Ryd$^{ex}$) with central frequency $E_g + 24$ Ryd$^{ex}$. Photon energies are $E_g + 24$ Ryd$^{ex}$(——), $E_g + 16$ Ryd$^{ex}$ (· · · · · ·), $E_g + 8$ Ryd$^{ex}$ (– – –), and $E_g$ (— — —).

time necessary for this Bose condensation to develop is estimated to be of the order of 100 ps (Inoue and Hanamura 1976a), and could not be covered by our calculation within the machine time allocated. However, the spontaneous excitonic polarization must have a component that is coherent with the initial seed polarization produced by the laser pulse, so that such a development of Bose condensation must be detected in the off-diagonal element of the Keldysh function.

Hoping to detect any such signs, we have solved the population dynamics with the phonon frequency reduced to 0.8 Ryd$^{ex}$, with the phonon bandwidth $\delta_D = 0.4$ Ryd$_{ex}$, and with the phonon temperature $T = 0$ in order to simulate the energy loss to acoustic phonons. The electron–phonon coupling is taken to be $\gamma(0, 0) = 3.0 \times 10^{-2}$ Ryd$^{ex}$. Figure 5 compares the time evolution of electron population density in the momentum space for two values of the pump laser amplitude $W_0 = 0.02$ Ryd$^{ex}$ and $W_0 = 0.20$ Ryd$^{ex}$. The pump laser energy is centred round $E_g$; the pulse envelope is taken to be a Gaussian function of band width $\delta_p = 1.0$ Ryd$^{ex}$ centred round $t_c = 2.0$ (Ryd$^{ex}$)$^{-1}$,

$$-\mu E(t) = W_0 \exp(-i\omega t) \exp\left[-\{\delta_p(t - t_c)\}^2\right]. \tag{48}$$

The time separation between two consecutive lines is 0.67 (Ryd$^{ex}$)$^{-1}$ in both figures. For the case of small laser amplitude $W_0 = 0.02$ Ryd$^{ex}$, the carriers are first created at a wide range of momentum by the pulsed laser. The population profile continues to evolve after the pump field has subsided, developing small bumps at larger momenta which then grow and move toward smaller values of $k$. It should be noted that the total number of electrons is conserved in this latter stage. This oscillatory evolution is largely due to the Coulomb

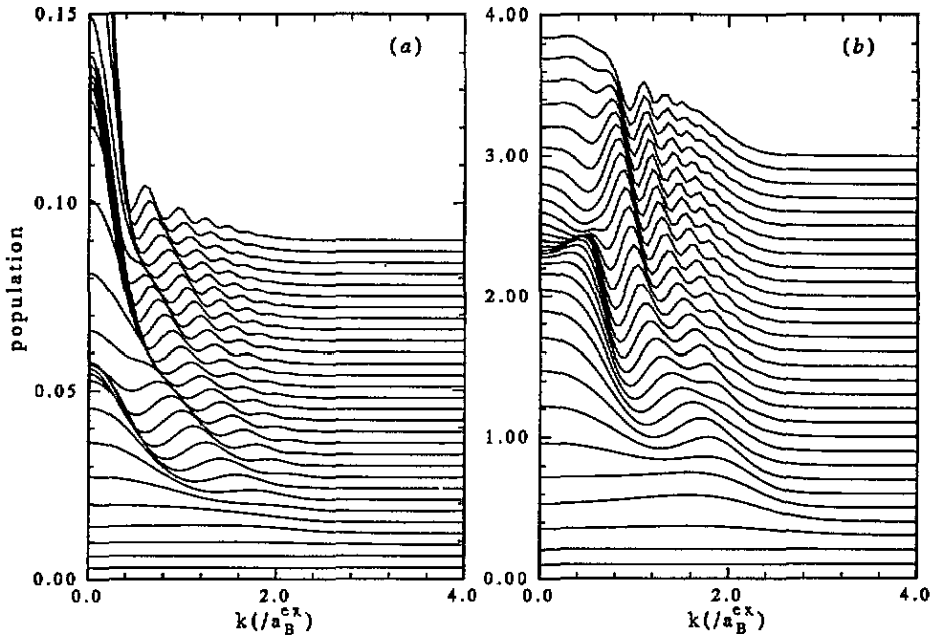


**Figure 5.** Temporal variation of electron population in $k$-space for pulse laser amplitude (a) $W_0 = 0.02$ Ryd$^{ex}$ and (b) $W_0 = 0.20$ Ryd$^{ex}$. The time separation of two consecutive curves is 0.671 (Ryd$^{ex}$)$^{-1}$.

exchange interaction among the carriers, as is indeed verified by doing the same calculation without the Coulomb interaction or the phonon interaction. The carrier density accumulates with time near the origin of the $k$-space after giving up energy to the cold phonon system. The oscillatory behaviour is highly non-linear with respect to pulse intensity and pulse duration, so that we have not been able to identify the oscillation frequency with any particular energy scale. For the case of large laser amplitude $W_0 = 0.2$ Ryd$^{ex}$, the electron population shows an even more complicated behaviour, again largely as a result of the Coulomb exchange interaction among the carriers. The carrier density develops a broad peak at small momentum, indicating a nearly semimetallic situation at large $t$. (Notice the population is approaching unity near the origin.)

In figure 6 we show the time evolution of the magnitude of polarization in the momentum space, in view of the interest in the quantity in fast-transient experiments such as four-wave mixing (see e.g. Schmitt-Rink *et al* 1991). All parameters are the same as in figure 5. After the laser pulse has passed, the general trend of the polarization is to diminish with time as carriers undergo phonon emission/absorption. The polarization also exhibits oscillatory behaviour nearly out of phase with that in figure 5. The behaviour is complex in contrast to the case of quantum phonon beat where the beat frequency is unambiguously identified with the phonon frequency (Tran Thoai and Haug 1993, Schilp *et al* 1994). For the case of $W_0 = 0.2$ Ryd$^{ex}$, the polarization decay is noticable at small $|k|$ as the carrier population builds up there. Significant structures remain in the region near the 'Fermi surface' where the occupation number is neither small nor large (i.e. approaches unity).

The process of energy loss can be seen in the frequency-resolved emission rate of incoherent luminescence as shown in figure 7(a) for $W_0 = 0.02$ Ryd$^{ex}$ and in figure 7(b) for $W_0 = 0.2$ Ryd$^{ex}$. The frequency resolution is taken to be $\delta_{res} = 1.0$ Ryd$^{ex}$ in both figures.

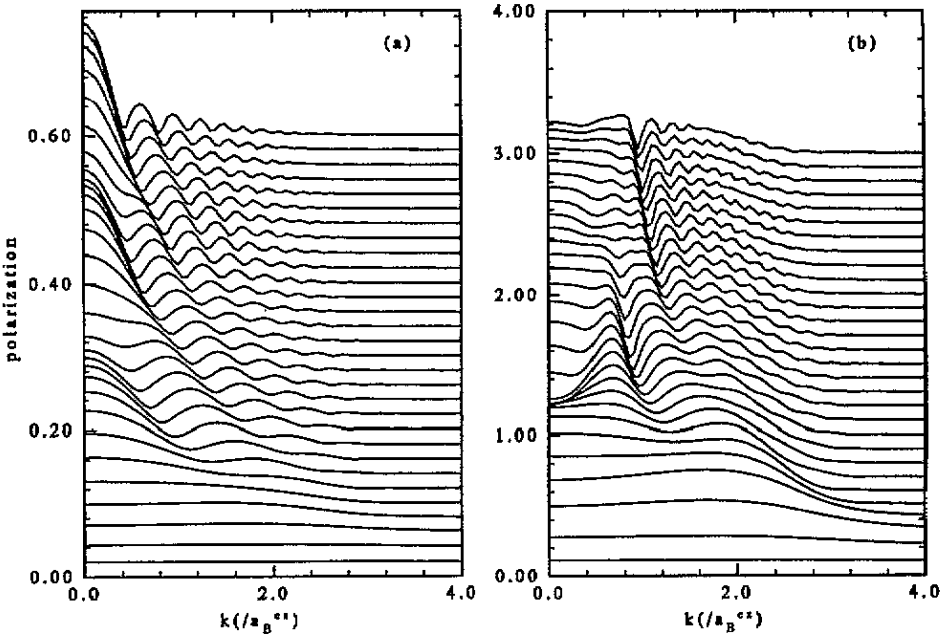


**Figure 6.** Temporal variation of the magnitude of electron–hole polarization in $k$-space for pulse laser amplitude (a) $W_0 = 0.02$ Ryd$^{ex}$ and (b) $W_0 = 0.20$ Ryd$^{ex}$. The time separation of two consecutive curves is 0.671 (Ryd$^{ex}$)$^{-1}$.

For the case of smaller laser intensity, the incoherent luminescence rate oscillates with time with a frequency of about 7 (Ryd$^{ex}$)$^{-1}$. The amplitude of this oscillation which is due to the Coulomb exchange interaction continues to grow even long after the pump laser pulse has subsided. The emission is strongest at around the frequency $E_g - 1.5$ Ryd$^{ex}$. The shift in excitonic level is dependent on the electron–phonon coupling, and is attributed to the band energy renormalization. The effect of energy exchange with phonons is seen in the increase of emission rate of lower-frequency photons relative to that of photons near $E_g$, although the emission peak shifts slightly towards the higher energy (see also figure 9(a)). The effect is more pronounced in the case of a stronger excitation $W_0 = 0.2$ Ryd$^{ex}$.

The frequency-resolved emission rate of coherent luminescence is shown in figure 8 for the case $W_0 = 0.02$ Ryd$^{ex}$. Initially, the rate closely follows the pump laser profile, but then persists with oscillation long after the excitation. The oscillation is of opposite phase to that of the incoherent luminescence, as is expected from the Coulomb exchange model. Although it cannot be determined from the present result whether the coherent luminescence grows with time, the persistent polarization will provide the nucleus for excitonic condensation. Finally, figure 9 compares the frequency dependence of coherent and incoherent emission rate at oscillation peaks for the cases of $W_0 = 0.02$ Ryd$^{ex}$ and $W_0 = 0.2$ Ryd$^{ex}$. Since the coherent and incoherent emissions correspond to exciton condensate recombination and quasiparticle recombination, respectively, the increased difference in the peak frequency for $W_0 = 0.2$ Ryd$^{ex}$ should correspond to a larger excitonic gap.

## 4. Concluding remarks

We have performed a quantum mechanical population dynamics calculation for the case of carrier excitation in a two-band semiconductor by a short laser pulse. The Dyson

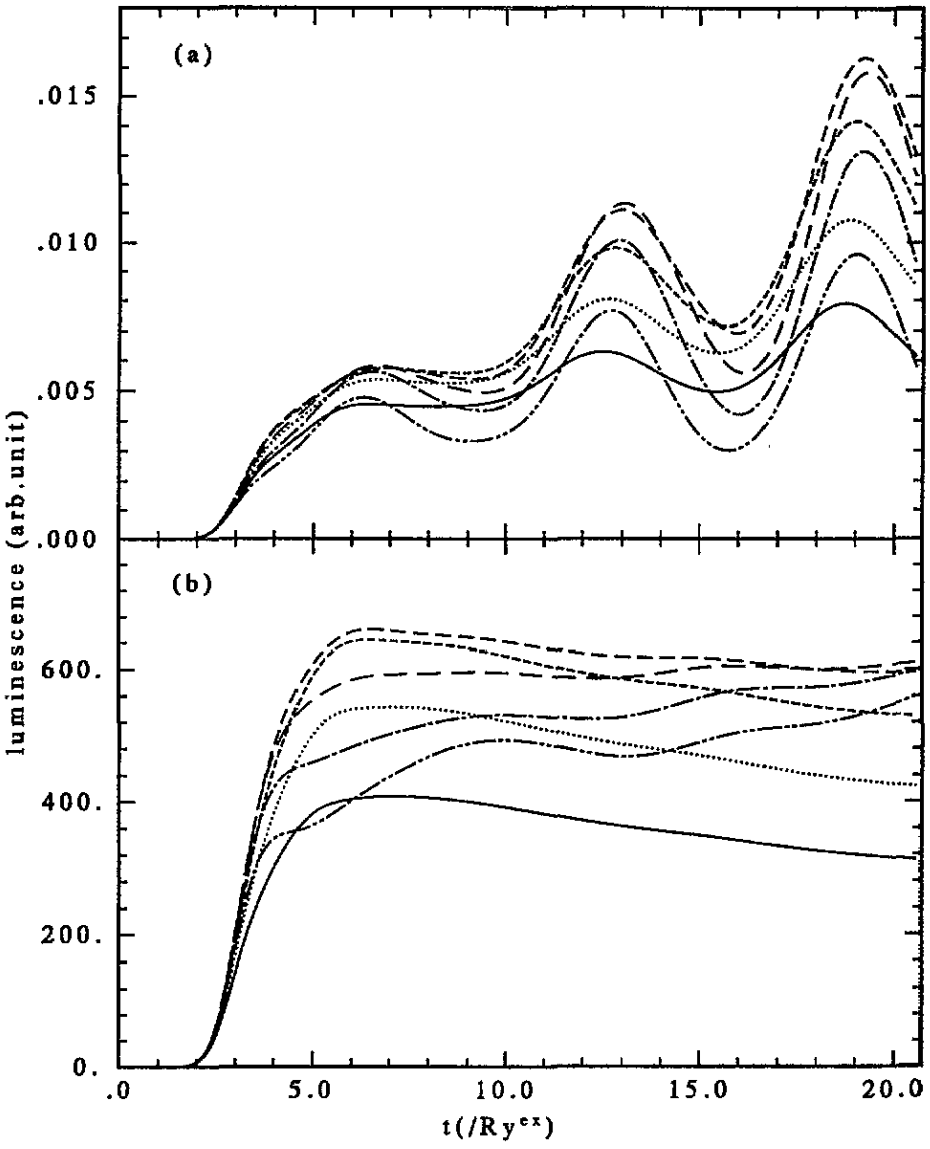


**Figure 7.** Frequency-resolved incoherent emission rates as functions of time. Pump pulse height, (a) $W_0 = 0.02$ Ryd$^{ex}$, (b) $W_0 = 0.20$ Ryd$^{ex}$. Photon energies, $E_g - 3.0$ Ryd$^{ex}$ (— · · —), $E_g - 2.5$ Ryd$^{ex}$ (— · —), $E_g - 2.0$ Ryd$^{ex}$ (— — —), $E_g - 1.5$ Ryd$^{ex}$ (– – –), $E_g - 1.0$ Ryd$^{ex}$ (----), $E_g - 0.5$ Ryd$^{ex}$ (· · · · · ·), and $E_g - 0.0$ Ryd$^{ex}$ (——). Frequency resolution $\delta_{res} = 1.0$ Ryd$^{ex}$.

equation is solved numerically, treating the two-point function as a matrix with time indices, thus avoiding making an *a priori* assumption as to the temporal behaviour of the Keldysh functions. The Coulomb interaction is treated in a Hartree–Fock approximation, while the electron–phonon interaction is treated up to the second order in the self-energy. The result for the temporal behaviour of luminescence intensity and red shift was in agreement with the experimental observation. The persistence of polarization function long after the pump light has subsided while the incoherent emission accumulates at lower energies at the same

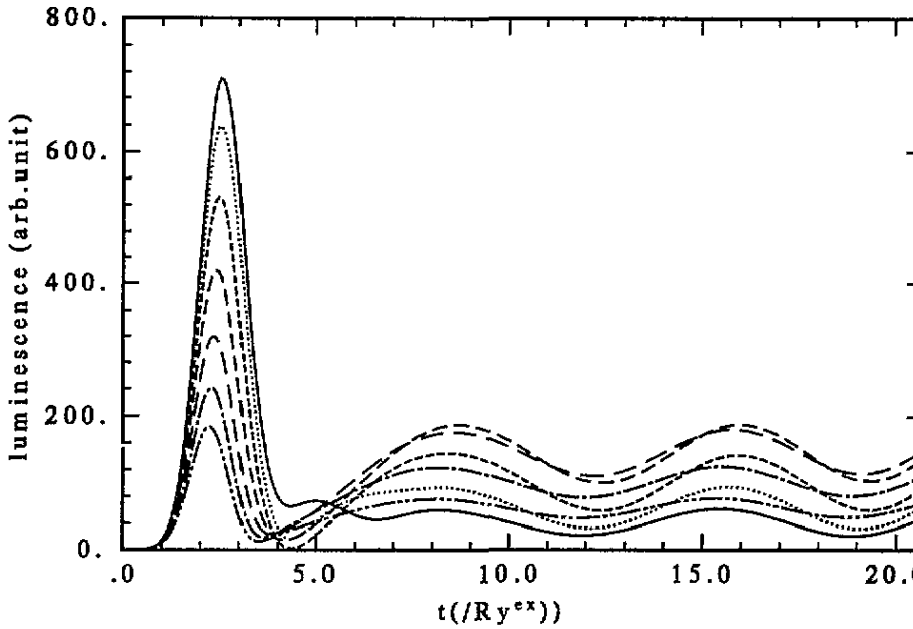


**Figure 8.** Frequency-resolved coherent emission rates as functions of time for pump laser amplitude $W_0 = 0.02$ Ryd$^{ex}$. Photon energies are $E_g - 3.5$ Ryd$^{ex}$ (— · · —), $E_g - 3.0$ Ryd$^{ex}$ (— · —), $E_g - 2.5$ Ryd$^{ex}$ (— — —), $E_g - 2.0$ Ryd$^{ex}$ (– – –), $E_g - 1.5$ Ryd$^{ex}$ (- - - -), $E_g - 1.0$ Ryd$^{ex}$ (· · · · · ·), and $E_g - 0.5$ Ryd$^{ex}$ (——). Frequency resolution $\delta_{res} = 1.0$ Ryd$^{ex}$.

time suggests the possibility of excitonic condensation.

The population dynamics has long been studied using the classical master equation with only the transition probability being derived with quantum mechanics. It has been difficult, therefore, to study the coherent properties and fast transient phenomena such as exciton condensation and quantum beats. Now, a quantum mechanical treatment of the transient population dynamics is becoming practicable as a result of the recent development in parallel computing. The present calculation is one such attempt, but still involves a number of approximations which may not be fully justified but are necessitated by the computational limitations. The Coulomb interaction will have to be treated beyond the Hartree–Fock approximation, as has been suggested by Rota *et al* (1993) based on the experimental observation of fast carrier thermalization. A treatment of Coulomb scattering at very short times in random phase approximation has been given by El Sayed *et al* (1994) who found a non-exponential decay of polarization

$$|\langle P_k(t)\rangle| = \exp\left\{-(t/\tau_G)^3\right\} \tag{49}$$

where $\tau_G$ is the non-exponential decay time. This applies to extremely short times when the retarded Green functions have not yet evolved. Omission of such an effect leaves the present calculation still a long way from a direct comparison with experiment, while a random phase approximation calculation for a general time scale along the lines of the present calculation will involve too massive a computation.

Coulomb scattering set aside, the second-order self-consistent treatment of the electron–phonon interaction in the self-energy diagram cannot be justified for a semiconductor in the same manner as for a metal. In materials such as $CuCl_2$, excitons are known to form excitonic molecules which Bose condense first as the carrier concentration is increased (see

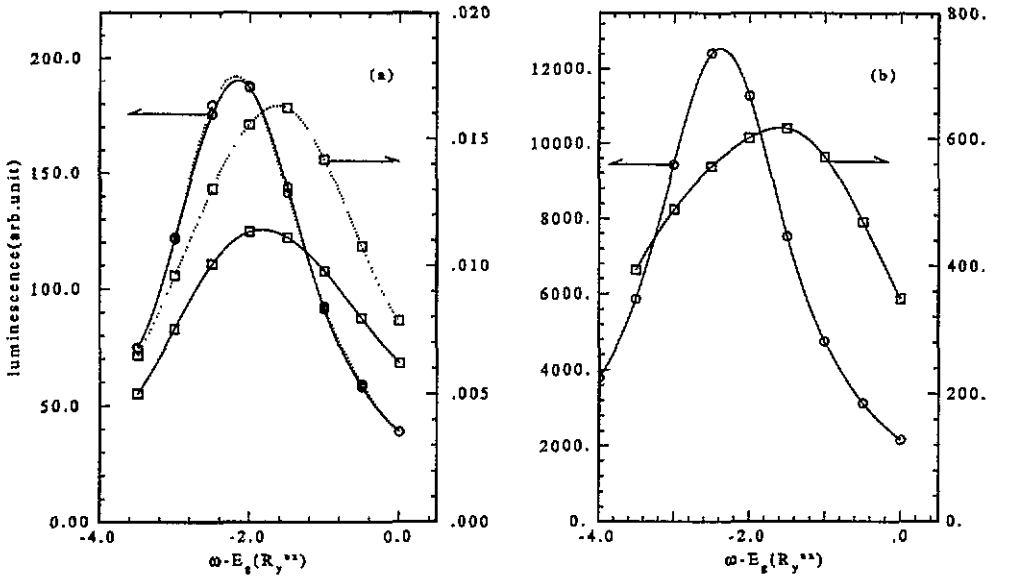


**Figure 9.** Frequency dependence of coherent (○) and incoherent (□) emission rate at various times for two values of laser amplitude $W_0$. (a) $W_0 = 0.02$ $Ryd^{ex}$, $t = 8.6$ $(Ryd^{ex})^{-1}$ (——), $t = 16.0$ $(Ryd^{ex})^{-1}$ (·····) for coherent emission, $t = 13.0$ $(Ryd^{ex})^{-1}$ (——), $t = 19.0$ $(Ryd^{ex})^{-1}$ (·····) for incoherent emission. (b) $W_0 = 0.20$ $(Ryd^{ex})^{-1}$; $t = 15.0$ $(Ryd^{ex})^{-1}$. Spline curves are a guide to the eye.

e.g. Peyghambarian *et al* 1983). A treatment of such a phase in the framework of Bogoliubov approximation will involve another set of order parameters to be solved simultaneously with the excitonic functions (see e.g. Inoue and Hanamura 1976b). An improvement on such points readily exhausts the computing capacity of any existing facility. Without such refinements, though, the numerical results presented here still have to be considered semiquantitative in confrontation with experimental data. Despite such shortcomings, the authors nevertheless hope to have demonstrated the growing feasibility of a realistic quantum mechanical treatment of such a complex problem as transient exciton population dynamics. When the computer capacity is futher increased, a more fundamental improvement may become feasible, e.g. solving the equations simultaneously also for four-point and higher-order functions, thereby relaxing the necessity of introducing decomposition assumptions such as the mean-field approximation.

## Acknowledgments

The authors acknowledge the opportunity offered by Fujitsu Laboratories Inc. to use the parallel computer AP1000 at Fujitsu Parallel Computing Research Facility (FPCRF) in the course of the numerical work. The authors also gratefully acknowledge the assistance given them by the staff of the facility, especially by Dr Sachiko Yamaki of Tsukuba Division and Dr Noriko Ikeda of FPCRF.

## References

Butov L V, Zrenner A, Abstreiter G, Bohm G and Weimann G 1994 *Phys. Rev. Lett.* **73** 304

Chemla D S, Miller D A B and Schmitt-Rink S 1987 *Optical Nonlinearities and Instabilities in Semiconductors* ed H Haug (New York: Academic) p 83
Eberly J H and Wodkiewitz K 1977 *J. Opt. Soc. Am.* **67** 1252
El Sayed K, Banyai L and Haug H 1994 *Phys. Rev.* B **50** 1541
Glutsch S and Zimmermann R 1992 *Phys. Rev.* B **45** 5857
Halperin B I and Rice T M 1968 *Solid State Physics* vol 21, ed H Ehrenreich and D Turnbull (New York: Academic) p 115
Hartmann M and Schäfer W 1992 *Phys. Status Solidi* b **173** 165
Haug H 1987 *Optical Nonlinearities and Instabilities in Semiconductors* ed H Haug (New York: Academic) p 53
Haug H and Koch S W 1990 *Quantum Theory of the Optical Electronic Properties of Semiconductors* (Singapore: World Scientific) p 339
Inoue M and Hanamura E 1976a *J. Phys. Soc. Japan* **41** 771
—— 1976b *J. Phys. Soc. Japan* **41** 1273
Keldysh L V 1965 *Sov. Phys.–JETP* **20** 1018
Khiznyakov V V and Rebane I K 1978 *Sov. Phys.–JETP* **47** 463
Knox W H, Fork R L, Downer M C, Miller D A, Chemla D S and Shank C V 1985 *Phys. Rev. Lett.* **54** 1306
Kuhn T and Rossi F 1992 *Phys. Rev.* B **46** 7496
Lifshitz E M and Pitaevskii L P 1981 *Physical Kinetics* (New York: Pergamon)
Peyghambarian N, Chase L L and Mysyrowicz A 1983 *Phys. Rev.* B **27** 2325
Rammer J and Smith H 1986 *Rev. Mod. Phys.* **58** 323
Rota L, Lugli P, Elsaesser T and Shah J 1993 *Phys. Rev.* B **47** 4226
Schäfer W 1987 *Optical Nonlinearities and Instabilities in Semiconductors* ed H Haug (New York: Academic) p 133
Schäfer W and Treusch J 1986 *Z. Phys.*B **63** 407
Schülp J, Kuhn, T and Mahler G 1994 *Phys. Rev.* B **50** 5435
Schmitt-Rink S and Chemla D S 1986 *Phys. Rev. Lett.* **57** 2752
Schmitt-Rink S, Chemla D S and Haug H 1988 *Phys. Rev.* B **37** 941
Schmitt-Rink S, Chemla D S and Miller D A B 1985 *Phys. Rev.* B **32** 6001
Schmitt-Rink S, Mukamel S, Leo K, Shah J and Chemla D S 1991 *Phys. Rev.* A **44** 2124
Stern F 1963 *Solid State Physics* vol 15, ed H Ehrenreich and D Turnbull (New York: Academic) p 372
Tran Thoai D B and Haug H 1993 *Phys. Rev.* B **47** 3574
Wake D R, Yoon H W, Wolfe J P and Morkoc H 1992 *Phys. Rev.* B **46** 13452
Yoon H W, Wake D R, Wolfe J P and Morkoc H 1992 *Phys. Rev.* B **46** 13461